On the Mechanism of CO_2 Reduction at Copper Surfaces: Pathways to C_2 Products

Alejandro J. Garza,[†] Alexis T. Bell,[*,‡] and Martin Head-Gordon[*,¶]

Joint Center for Artificial Photosynthesis, Lawrence Berkeley National Laboratory, Berkeley, California 94720, USA, Department of Chemical and Biomolecular Engineering, University of California at Berkeley, Berkeley, California 94720, United States, and Department of Chemistry, University of California at Berkeley, Berkeley, California 94720, United States

E-mail: alexbell@berkeley.edu; mhg@cchem.berkeley.edu

Abstract

Based on constraints from reported experimental observations and density functional theory simulations, we propose a mechanism for the reduction of CO_2 to C_2 products on copper electrodes. To model the effects of an applied potential bias on the reactions, calculations are carried out with a variable, fractional number of electrons on the unit cell, which is optimized so that the Fermi level matches the actual chemical potential of electrons (*i.e.*, the applied bias); an implicit electrolyte model allows for compensation of the surface charge, so that neutrality is maintained in the overall simulation cell. Our mechanism explains the presence of the seven C_2 species that

[*]To whom correspondence should be addressed

[†]Joint Center for Artificial Photosynthesis, Lawrence Berkeley National Laboratory, Berkeley, California 94720, USA

[‡]Department of Chemical and Biomolecular Engineering, University of California at Berkeley, Berkeley, California 94720, United States

[¶]Department of Chemistry, University of California at Berkeley, Berkeley, California 94720, United States

have been detected in the reaction, as well as other notable experimental observations. Furthermore, our results shed light on the difference in activities toward C_2 products between the (100) and (111) facets of copper. We compare our methodologies and findings with those in other recent mechanistic studies of the copper-catalyzed CO_2 reduction reaction.

Keywords

Artificial Photosynthesis, DFT, Electrocatalysis, Mechanisms, Ethanol, Ethylene

Introduction

Copper is unique among metals in its ability to catalyze the electrochemical reduction of CO_2 to hydrocarbons, alcohols, and other organic products containing up to three carbon atoms.[1–3] The major C_2 products of the copper-catalyzed CO_2 reduction reaction (CO_2RR) are ethylene and ethanol, both of which have considerable value for the chemical and fuels industries. For example, ethylene can be used as a feedstock for producing chemical intermediates, *e.g.*, ethylene oxide, polyethylene, and diesel (via ethylene oligomerization), whereas ethanol is also a chemical feedstock (*e.g.* for ethene, glycol ethers, amines and esters), a solvent, and a fuel. Product selectivity using copper remains an issue, though, since experimental studies have shown that the CO_2RR on Cu produces H_2 and a variety of C_1, C_2, and C_3 products, as well as ethylene and ethanol.[3] It has also been observed that the ratio between C_1 and C_2/C_3 products is strongly affected by surface morphology of Cu.[4–6] In particular, the more open Cu(100) surface exhibits greater selectivity to products with C-C bonds than the close-packed Cu(111) facet. It is also notable that Cu-based catalysts require high overpotentials to achieve significant selectivity to ethylene and ethanol, and minimal selectivity to H_2, $HCOO^-$, and CH_4.[3,7–10] These considerations have motivated an interest in identifying possible mechanisms for the CO_2RR and the elementary steps that control the

products distribution.

Experimental studies of the mechanism of the CO_2RR have been challenged by difficulties in carrying out spectroscopic observations of adsorbed reactants and intermediates. While in-situ IR spectroscopy has offered some insights into the nature of adsorbed CO_2, CO, and formate,[11,12] this approach has not been successful in identifying the surface species that are critical to the formation of observed reaction products, particularly those containing two or more carbon atoms. Greater mechanistic insights have come from analyzing the products formed when postulated intermediates are fed and allowed to undergo electrochemical reduction, *e.g.*, CO, acetaldehyde, glyoxal, *etc.* The subsequent observation of products of CO_2 reduction is taken as evidence that the compound may indeed play a role in the mechanism. Schouten *et al.*[13] have used this approach to deduce a rough mechanism for the CO_2RR. It should be noted, though, that the mechanism proposed by these authors is not complete, since it does not include pathways to all of the CO_2 reduction products that have been observed (*e.g.*, ethanol and glycolaldehyde).[3] Additionally, the technique of feeding proposed reaction intermediates has two significant limitations. The first is that only stable molecular compounds can be investigated. The second drawback is that a reactant yielding products of CO_2 reduction is a necessary, but not sufficient, condition for the reactant to be an intermediate.

A sufficient condition for a species to be an intermediate is that the path involving such an intermediate is thermodynamically and kinetically favored over all alternative paths under CO_2RR conditions. This is where theoretical calculations of free energy changes along a proposed pathway provide information not accessible from experiments. It should be noted, though, that approximate methods are necessary for modeling systems that are as complex as the CO_2RR, which can result in errors in the estimated free energies of the elementary steps considered, and could, therefore, lead to erroneous conclusions. However, the predictions made on the basis of theoretical analysis can be validated (or invalidated) by comparison with experimental observation in order to fill in the missing pieces in the puzzle of the CO_2RR

mechanism. The more observables that a given mechanism can account for, the more likely it is to be physically meaningful.

This paper describes our efforts to develop a mechanism for the CO_2RR on copper with the aim of identifying elementary steps leading to the C_2 products seen experimentally, and explaining the difference in activities between the (100) and (111) facets of Cu. As a part of this effort we have calculated the free energies for each elementary step from first principles using density functional theory (DFT) and a model of the double layer potential at the cathode. We place greater emphasis on the Cu(100) surface because, as noted above, this surface exhibits a high selectivity for C_2 products. Our decision to limit this study to the formation of C_2 products is based on two main considerations. First, the mechanism for forming C_1 products is less complex (*i.e*, there are fewer possible reactions) and has been investigated extensively.[9,10,13–17] By contrast, less effort has been devoted to understanding the formation of C_2 products, apart from the question of C-C bond formation.[16–22] Second, ethylene and ethanol are high value targets which are already produced in substantial amounts by existing techniques.[27–29]

There have been a number of earlier mechanistic studies of the electrochemical reduction of CO_2 on copper based on theoretical analysis of the energetics of possible reaction pathways.[13–22] The results reported here differ from those reported previously in that, to the best of our knowledge, this is the first study in which a full mechanism for all the seven C_2 products reported in the literature[3]—ethylene, ethanol, acetaldehyde, ethylene glycol, glycolaldehyde, glyoxal, and acetate—are included and the free energy landscape for forming these products is analyzed. Our study does not consider the possible role of subsurface oxides,[23,24] and surface defects,[25] either of which, if present, could potentially provide additional pathways. Following Occam's Razor, our objective is to establish as much as we can about the mechanism in the absence of any chemical or physical modifications to the (100) and (111) copper surfaces.

Our study is also differentiated from past work on pathways to C_2 products by the

methodology employed for the simulations. Specifically, we use an implicit electrolyte model which allows us to better simulate the effect of an applied voltage by varying the charge on the surface so that the Fermi level matches the target chemical potential of electrode electrons.[21,26] This methodology for modeling electrochemical reactions at surfaces, which we refer to as the constant electrode potential (CEP) model, was recently used by our research group to study the initial steps of the CO_2RR on Cu(100).[21] We expand upon this work and compare our approach and findings with those from previous theoretical studies.

Theory and Methods

Computational details. All calculations were carried out with the Vienna *Ab initio* Simulation Package[30] (VASP) using the revision of the Perdew–Burke–Ernzerhof functional proposed by Hammer *et al.*[31] (RPBE). The surface unit cell was represented by three layers of eight Cu atoms with a spacing between images along the surface normal that is greater than 20 Å. A $4\times4\times1$ Monkhorst–Pack mesh was used for **k**-point sampling of the Brillouin zone. All geometries were fully optimized with a plane wave energy cutoff of 500 eV; the electronic energy and forces were converged to within 1×10^{-6} eV and 0.01 eV/Å, respectively. Transition state searches were performed using the climbing image nudged elastic band[32,33] and dimer[34] methods. The electrolyte was incorporated implicitly with the Poisson–Boltzmann model implemented in VASPsol.[35–37] The relative permitivity of the media was chosen as $\epsilon_r = 78.4$, corresponding to that of water; the concentration of the electrolyte was set to 0.1 M, equivalent to a Debye length of 9.61 Å. These setting are intended to mimic typical reaction conditions.[16]

Vibrational frequencies of the adsorbates were calculated for the (electrolyte) optimized structures in order to obtain thermal corrections to the free energy at 300 K; the formulas for the zero-point energy, enthalpic, and entropic corrections used here can be found in Ref. 26. To account for the suppression of translational and rotational motions of the solute

by the solvent,[38] we neglected entropic contributions from these movements. This approach improves agreement with experiment for free energies of bimolecular reactions in solution.[38,39] We treated all degrees of freedom of the adsorbate as vibrational and assumed no significant change in surface vibrations. Unusually low vibrational modes (< 50 cm^{-1}) were reset to 50 cm^{-1}. This protocol provides consistency with previous work by our research group.[21]

Potential dependence models. We consider—for reasons that will be explained later—two models for taking into account the effect of applied potential (U) on free energies (ΔG) and activation free energies ($\Delta G^{\ddagger}$): the computational hydrogen electrode[40] (CHE) model, and the fixed or constant electrode potential (CEP) model.[21] The CHE takes advantage of the fact that the reaction

$$\mathrm{H}^{+}_{(\mathrm{aq})} + e^{-} \rightleftharpoons \frac{1}{2}\mathrm{H}_{2(\mathrm{g})}, \tag{1}$$

is equilibrated at 0 V *vs* the reversible hydrogen electrode (RHE) at all pH values. Using the relationship between the chemical potential of electrons and the potential U, $\mu(e^{-}) = eU$, with e as the (positive) elementary charge, the change in free energy for the reaction

$$\mathrm{A} + \mathrm{H}^{+}_{(\mathrm{aq})} + e^{-} \longrightarrow \mathrm{AH} \tag{2}$$

is therefore

$$\Delta G(U) = \mu(AH) - \mu(A) - \left[\frac{1}{2}\mu(\mathrm{H}_{2(g)}) - eU\right]. \tag{3}$$

The CHE can be adapted to calculate potential-dependent energy barriers by considering a two-step process consisting of a reductive adsorption[41]

$$\mathrm{A}^{*} + \mathrm{H}^{+}_{(\mathrm{aq})} + e^{-} \longrightarrow \mathrm{A}^{*} + \mathrm{H}^{*}, \tag{4}$$

where the asterisk denotes an adsorbed species, and a chemical reaction on the surface

$$\mathrm{A}^* + \mathrm{H}^* \longrightarrow \mathrm{AH}^*. \tag{5}$$

The activation energy is then

$$\Delta G^{\ddagger}(U) = \Delta G^{\ddagger}(U_0) + e\beta(U - U_0), \tag{6}$$

where U_0 is the equilibrium potential for the reductive adsorption step in Eq. 4, and β the reaction symmetry factor. Here, we approximate $\beta = 0.5$ which is a reasonable assumption based on the fact that, from the data available in the Supporting Information of Ref. 16, we computed the average value of β—estimated with a more sophisticated approach based on dipole moments—for 36 reactions related to CO_2 reduction on copper as 0.49 (with a median of 0.49 and a standard deviation of 0.04).

Approaches based on the CHE are computationally convenient and have been useful in predicting properties such as redox potentials and catalytic activities.[26] However, they neglect the effect of the surface charge on the structures and stabilities of adsorbates. The CEP model addresses this issue via a self-consistent procedure in which the number of electrons in the unit cell is altered and allowed to be fractional so that the Fermi level, E_F, matches the electrode potential. In other words, iterative DFT calculations with varying number of electrons are carried out in electrolyte media until satisfaction of the equality

$$U = \frac{-E_F - \phi_{\mathrm{SHE}}}{e}, \tag{7}$$

where $\phi_{\mathrm{SHE}} = 4.43$ eV is the RPBE value of the thermodynamic work function of the standard hydrogen electrode.[44] Thus, in accordance with its definition, the Fermi level equals the chemical potential of electrons (as explained in Ref. 21, in this model, E_F is the energy difference between an electron in the electrode and one in vacuum). The problem of having

a charged unit cell is avoided because the electrolyte charges from the Poisson–Boltzmann model compensate for the excess of electrons to maintain neutrality in the overall system. The change in free energy for the reaction A $\longrightarrow$ B can then be calculated as the difference in chemical potential between A and B plus the mass conservation terms[26]

$$\begin{aligned}\Delta G(\mathrm{A} \longrightarrow \mathrm{B}) =& \mu(\mathrm{B}) - \mu(\mathrm{A}) - \mu_e(N_e^{\mathrm{B}} - N_e^{\mathrm{A}}) \\ & -\mu_+(N_+^{\mathrm{B}} - N_+^{\mathrm{A}}) - \mu_-(N_-^{\mathrm{B}} - N_-^{\mathrm{A}}),\end{aligned} \tag{8}$$

where μ_e is the chemical potential of electrons (the Fermi energy), N_e^{A}, N_+^{A}, and N_-^{A} the number of electrons, cations, and anions in A, respectively, and $\mu_\pm$ the chemical potential of the ions. The latter is estimated as[42,43]

$$\mu_\pm = kT \ln \frac{c_b a^3}{1 - 2c_b a^3} \tag{9}$$

with c_b as the bulk concentration of ions (set here as 0.1 M), and a the ion radius. We assume the electrolyte to be $KHCO_3$ and use tabulated ion radii[45,46] for K^+ (152 pm) and HCO_3^- (156 pm) to compute $\mu_\pm$. The pH value is set to 7 in our simulations. For reduction processes, reactions were modeled as $\mathrm{A}^* + \mathrm{H_2O} + e^- \longrightarrow \mathrm{AH}^* + \mathrm{OH}^-$ in order to compute ΔG values with the CEP. Accurately computing the solvation energy of the hydroxide ion is challenging for implicit solvation models, specially under periodic boundary conditions[47] (the error is on the magnitude of 1 eV). Therefore, we use the value of -4.53 eV for the solvation energy of the OH^- anion, which was determined from first-principles calculations and is in agreement with experimental measurements.[48] From our own calculations, the error in the solvation energy of water computed with the RPBE functional in VASPsol is less than 0.01 eV. Consequently, our results are not affected by the use of experimental, rather than theoretical, solvation energies for calculating the free energy of H_2O.

Having discussed the CHE and CEP models, their advantages and disadvantages become clear. The CHE permits one to estimate ΔG and $\Delta G^\ddagger$ at any potential without any increase

in computational effort over standard DFT free energy calculations; the drawback is the neglect of more specific effects of the potential (*e.g.*, the surface and electrolyte charge). The CEP can take into account these effects, at an increased computational cost because of the need for iterative DFT calculations at each value of the applied bias. Hence, we report most CEP results only at -1 V *vs* the RHE, which is representative of typical reaction conditions, and use the CHE to estimate effects at other potentials. Since, to the best of our knowledge, the CEP has not been extensively used to model the CO_2RR, unlike the widely employed CHE, we discuss the key differences between results obtained by the two models as they arise, and point out possible pitfalls of ignoring the surface charge.

Comparison with methodologies used in previous studies. In what follows, we compare our results with those of Cheng *et al.*[17] and Luo *et al.*[16] We thus discuss here the differences in the methodologies used in these studies and that employed here. Luo *et al.*[16] use the PBE functional, one to three water molecules as solvent, and the CHE to estimate the effects of an applied potential. Cheng *et al.*[17] also employ the PBE functional, but with five layers of explicit water and a constant charge (variable potential) capacitor-like model for the applied potential.[17,59] Thus, neither of these studies includes the surface or electrolyte charges that are present at a constant electrode potential. In addition, the capacitor model assumes the dipole moment of the adsorbates to be small,[59] which is not true for many of the possible intermediates of the CO_2RR. Although our use of implicit solvation and electrolyte charges is an approximation to explicit solvent models, DFT molecular dynamics calculations of a charged surface in 0.1 M aqueous solution are not practical with current technology: a calculation on a system of about 100 Å of electrolyte would be required to attain sufficient screening of the electrostatic field from the surface in the environment.[26] Moreover, the number of electrons in the unit cell required to match the applied potential depends on the choice of the unit cell itself and is, in general, fractional. Thus, a fractional electrolyte charge is also required to maintain neutrality in the solid-liquid interface. Lastly, based on our experience, the choice of the functional, PBE versus RPBE, does not significantly affect

most reaction energies. However, exceptions arise when adsorption/desorption processes are involved, where we usually find that RPBE yields more reasonable results (examples of this are given below). Indeed, the motivation for revising PBE into RPBE was to improve the description of adsorption energies.[31]

Results and Discussion

The mechanism we propose for the reduction of CO_2 to C_2 products is shown in Fig. 1. Before discussing how this mechanism was developed and how it differs from those proposed previously, we define our conventions and notation. In Fig. 1 and throughout this work, free energies (always in eV) excluding the effects of applied potential (at 0 V *vs* RHE using the CHE) are written next to reaction arrows; those computed at -1 V using the CEP are highlighted in bold. This choice of showing ΔG values at $U = 0$ V using the CHE, and those at $U = -1$ V using the CEP, allows for straightforward comparison of both models at $U = -1$ V because the energy of electrochemical reactions changes linearly with U for the CHE. Cases where surface charge is important are also easy to identify with this convention. We also use solid and hollow arrows to represent exergonic and endergonic reactions, respectively, at 0 V *vs* the RHE. Unless otherwise stated, results presented are for the Cu(100) surface. Lastly, our reference electrode is the RHE and, as is customary, we refer to large, negative potentials as "high" potentials.

Our mechanism focuses on CO, rather than CO_2, as a starting point. It has been determined that CO_2 is converted to CO before undergoing further reduction; electroreduction of CO results in the same product distribution as that of CO_2.[13,49–51] (Furthermore, the pathway from CO_2 to CO is better established than that from CO to C_2 compounds and has been studied extensively.[8,9,15,16,52]) Hence, we study exclusively the mechanism of CO reduction, as this process determines selectivity in the CO_2RR; previous studies have taken a similar approach.[15,16,21] The very first reaction step (not shown in Fig. 1) to consider is therefore

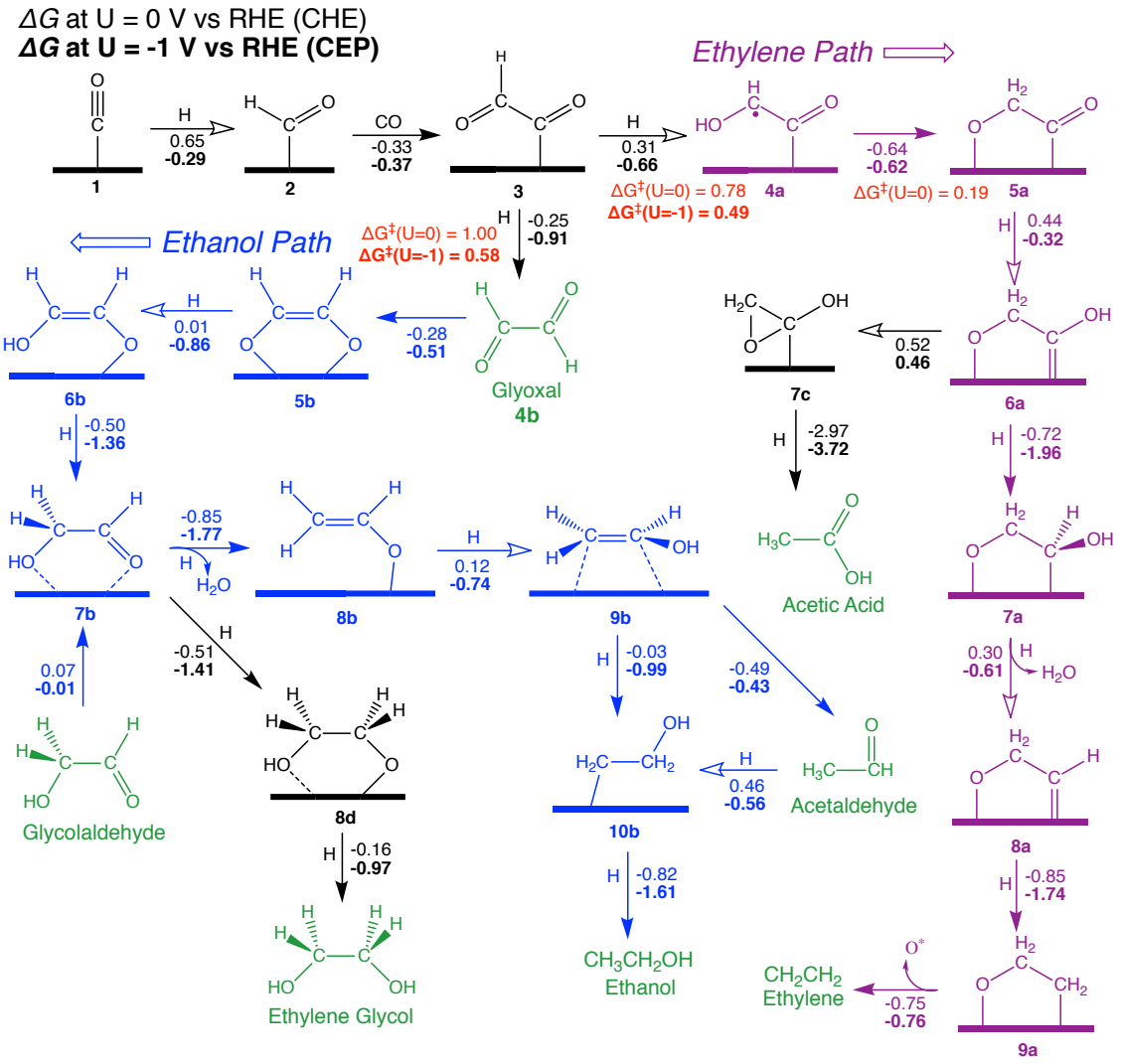

Figure 1: Proposed mechanism for the reduction of CO to C_2 products at high potentials on Cu(100). Calculated free energies (eV) are the numbers parallel to reaction arrows, where ΔG values at $U = 0$ V using the CHE appear in standard font (steps involving $H^+ + e^-$ can be corrected to $U = -1$ V by subtracting 1 eV). ΔG values at $U = -1$ V using the CEP (at pH = 7) appear in bold font. The seven C_2 products of CO_2 reduction on copper are highlighted in green. Calculated free energy barriers (eV) are provided for the critical reductive step from intermediate **3** to either **4a** or **4b** that determines selectivity between the pathway to ethylene (purple) and ethanol (blue).

the adsorption of CO on the Cu(100) surface. The calculated RPBE adsorption energy (in the absence of an applied potential) of −0.59 eV compares well with the experimental value of −0.57 eV.[53] At −1 V *vs* the RHE (from the CEP), the binding becomes stronger (−0.75 eV) due to charge donation from the surface to the empty π^* orbital of CO, which is more localized on the carbon atom. The moderate adsorption energy of CO on copper is important as it enables its activation for further reduction and C-C bond formation, which does not occur in other metals that bind CO either too weakly or too strongly to make it reactive (Sabatier principle).

C-C bond formation. The two next steps, $^*\mathrm{CO} + \mathrm{H} \longrightarrow {}^*\mathrm{CHO}$ and $^*\mathrm{CHO} + \mathrm{CO} \longrightarrow {}^*\mathrm{COCHO}$ (see Fig. 1), are worth discussing in detail. Calle-Vallejo and Koper[18] proposed CO dimerization as the first step towards C_2 products. Cheng *et al.*[17] built upon this idea to devise a more complete mechanism in which CO dimerization is followed by hydrogenation of an oxygen atom ($^*\mathrm{COCO} + \mathrm{H} \longrightarrow {}^*\mathrm{COCOH}$). However, using the CEP model, Goodpaster *et al.*[21] have found that at high potentials (*i.e.*, $U \approx -1$ V, typical of experimental conditions) the reduction of CO to *CHO followed by reaction with *CO to form *COCHO was favored over *CO dimerization and subsequent reduction. The structures of *COCOH (**3'**) and *COCHO (**3**) are tautomeric; nonetheless, unlike the former, the structure of the latter does not involve a double bond to the surface (Scheme 1) or a free radical on the C atom. Consistent with those considerations, we calculated **3** to be 0.43 eV more stable than **3'** in the absence of an applied potential. This value increases to 0.75 eV at $U = -1$ V due to destabilization of the C=Cu double bond by the surface charge. Although explicit water molecules could provide more stabilization for **3'** relative to **3** due to **3'** being able to form an additional H-bond, theoretical studies suggest that explicit electrolyte ions favor the formation of aldehyde- and ketone-like adsorbates rather than alcohols.[54] Moreover, a resonance structure of **3** placing positive charge on the C atom bonded to Cu and negative charge on the adjacent O atom would be able to form stronger H-bonds than **3'**, while the destabilization due to placing charge on the C atom would be partially offset by the negative

applied voltage.

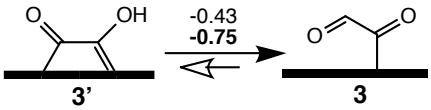

Scheme 1: Tautomerization of *COCHO.

The pH dependence of the CO_2RR suggests that, because ethylene formation is pH-dependent on the RHE scale (or, alternatively, pH-independent on the SHE scale), the rate determining step does not involve a proton.[55] For the CO $\longrightarrow$ CHO $\longrightarrow$ COCHO path, C-C bond formation is the rate determining step,[21] thus satisfying the observed pH dependence. For CO dimerization followed by reduction (CO $\longrightarrow$ COCO $\longrightarrow$ COCOH), the C-C coupling step is rate limiting too, and hence this reaction is also pH insensitive. This is also the case if a CO $\longrightarrow$ COH $\longrightarrow$ COCOH sequence is considered.[16] Therefore, all three of these mechanisms for C-C bond formation satisfy the experimentally observed pH dependence.

However, the observed potential and facet dependence of the CO_2RR provides additional conditions that can help distinguish between the possible mechanisms. Experiments indicate that ethylene and methane share a common intermediate on Cu(111) and at high potentials on Cu(100); whilst ethylene formation proceeds by a distinct path at low potentials on Cu(100).[56–58] Thus, we next report our investigations of the potential and facet dependence of C-C bond formation to propose a model that can explain these observations.

Figure 2 shows the variation in free energy with voltage for the reaction $^*\mathrm{CO} + \mathrm{CO} \longrightarrow {}^*\mathrm{COCO}$ on Cu(100) and Cu(111). At moderate potentials ($U \approx -0.5$ V) the reaction free energy is close to zero ($\Delta G \approx 0.05$ eV). This makes the formation of *COCHO via *COCO thermodynamically favorable around -0.37 V $< U < -0.65$ V (see Fig. 3). Only at about $U < -0.65$ V is *CHO predicted to be more stable than *COCO. In contrast, on the Cu(111) surface, *COCO is highly unstable compared to its components at all the calculated potentials (in fact, the geometry optimizations with the CEP method resulted in the two separate CO adsorbates; the structure in Fig. 2 is fixed from a calculation on a

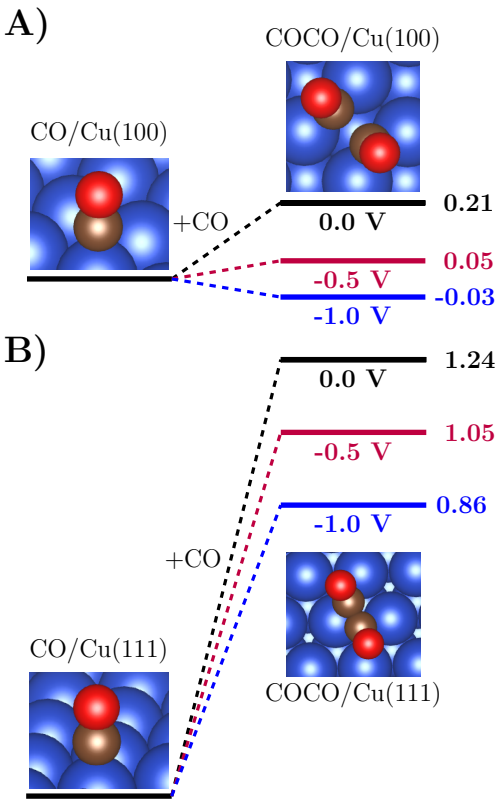

Figure 2: Free energy diagrams for CO dimerization on (A) Cu(100) and (B) Cu(111) surfaces at various potentials (*vs* the RHE at pH = 7) calculated using the CEP model. Reaction free energies are in eV.

neutral surface). Although an applied negative voltage stabilizes the CO dimer, the ΔG to generate *COCO is still 0.86 eV at $U = -1$ V (compared to 1.38 eV at $U = 0$ V and 1.05 eV at $U = -0.5$ V). However, the $\Delta G = 0.60$ eV for the reduction of *CO to *CHO on Cu(111) is slightly lower than on Cu(100).

The picture for C-C bond formation that emerges from these calculations is shown in Fig. 3. On Cu(100) at low potentials, *CO dimerizes and is then reduced to *COCHO, leading to C_2 products. On Cu(100) at high potentials and on Cu(111) at all potentials, *CO reduces to *CHO, which can lead to both methane as well as C_2 products. The experiments by Schouten *et al.*[56] show the appearance of methane and ethylene at (approximately) $U < -0.4$ V on Cu(111), ethylene at $-0.7 < U < -0.4$ V on Cu(100), and methane and ethylene at $U < -0.8$ on Cu(100). At the lower potentials, products are formed in larger amounts on Cu(100) than on Cu(111).[56] The pathways in Fig. 3 are consistent with these observations: Based on the CHE and assuming that *COCHO leads to C_2 products, the onset potential to generate ethylene on Cu(100) via the *COCO pathway is -0.36 V. On Cu(111), formation of *COCHO becomes thermodynamically favorable at -0.48 V, but has to go through the *CHO path that is higher in free energy at low potentials, leading to poor efficiencies at these potentials. At potentials more negative than about -0.65 V the *CHO path is thermodynamically favorable over the CO dimer path on both facets of copper; *CHO is therefore the common intermediate between ethylene and methane that experiments indicate to be present on Cu(111) and at high potentials on Cu(100).[56–58] The CEP calculations by Goodpaster *et al.*[21] showing that the kinetic barrier for CO dimerization on Cu(100) increases with an increasingly negative voltage, and vice versa for *CHO formation, furthermore support the mechanism in Fig. 3 and explain why the ethylene pathway closes at intermediate potentials on Cu(100).[56]

Based on the calculations by Li *et al.*[61] the reason why CO dimerization occurs on Cu(100) but not on Cu(111) may be attributed to the square symmetry of the former, although the lower coordination number on Cu(100) may also influence the stability of the dimer. We find that the preferred geometry for *COCO on Cu(100) has the C atoms adsorbed on

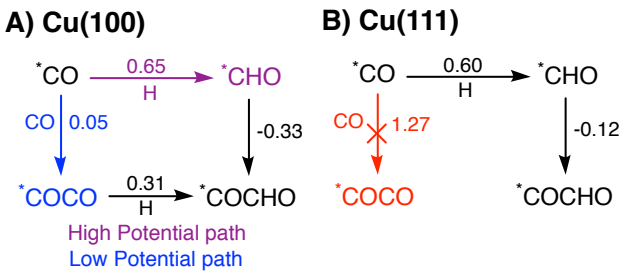

Figure 3: Paths to C−C bond formation and *COCHO on Cu(100) and Cu(111). Numbers next to reaction arrows are free energies in eV at 0 V *vs* the RHE according to the CHE.

bridge sites and linked to each other over a hole site (Fig. 2A), which is rather large due to the low coordination number of Cu. Such a structure is not possible on Cu(111), forcing the CO dimer to adopt a less stable geometry with a shorter C−C bond length (Fig. 2B). An alternative theory that allows for CO dimerization on Cu(111) is that subsurface oxide species promote CO_2 activation[23] and CO dimerization.[24] However, other experiments[62–64] as well as the Pourbaix diagram of Cu[65] suggest that no oxides are present near the surface under CO_2RR conditions. A more recent study attributes the enhanced activity of certain oxide-derived Cu catalysts to surface defects, rather than the presence of oxides.[25]

There is also the possibility of reducing *CO to *COH, rather than *CHO. Different studies have reached different conclusions on this question, depending on the computational techniques employed. In gas-phase CHE calculations, Nie *et al.*[52] found that *COH was favored; the opposite trend was encountered in explicit solvent[14] and CEP[21] simulations. Akhade *et al.*[54] found that the presence of adsorbed K^+ ions increases the selectivity for reducing *CO to *CHO by stabilizing these species and destabilizing the transition state to form *COH. According to our CEP calculations, the stability of *COH depends on the adsorption site: on a hole site of a Cu(100) surface, *COH is very close in energy (< 0.1 eV difference) to *CHO at all potentials between 0 and −1.0 V *vs* the RHE. However, on a top Cu(100) site (the preferred adsorption site of CO[66]) *COH is 1.2 and 1.4 eV higher in energy than *CHO at -0.5 and -1.0 V *vs* the RHE, respectively. These considerations along with the fact that C-C bond formation leads to either *COCHO or *COCOH, and that the former is

much more stable than the latter (specially at high potentials; see Scheme 1), suggest that *COCHO is the key intermediate in the conversion of CO_2 to C_2 compounds. Interestingly, recent experiments have identified infrared signals at 1584 and 1191 cm^{-1} from a possible CO_2RR intermediate,[67] and we calculated *COCHO to have infrared-active vibrations at 1526 and 1291 cm^{-1}. We should mention that Pérez-Gallent *et al.*[67] concluded that the observed signals originated from *COCOH because they calculated that *COCHO should have no IR signals in the range 1500–1600 cm^{-1}; however, the vibrational frequencies of the adsorbates depend strongly on their adsorption mode, and the *COCHO structure that we calculated as most stable has signals in the observed range. (It must also be noted that these IR measurements were carried out at potentials of +0.1 to −0.2 V *vs* RHE, which are significantly more positive than those of typical CO_2RR conditions.) Furthermore, the observation of glyoxal as minor reaction product[3] and likely intermediate[13] all but proves that *COCOH is present during the reaction.

A noteworthy experimental observation concerning C-C bond formation is the cation effect: larger ions promote the formation of C_2 products.[68,69] The CEP model contains dependence on the ionic radius of the cations due to the chemical potential of the ions entering the free energy expression in Eq. 8 (see also Eq. 9). Although small, the CEP model predicts a qualitatively correct cation effect: *COCO and *COCHO are stabilized by −0.02 and −0.002 eV, respectively, when considering Cs^+ as counterion as opposed to Li^+. Albeit important in determining C_1/C_2 selectivity, a detailed study of the cation effect is beyond the scope of the present paper. Nonetheless, the results of Resasco *et al.*[69] suggest that this effect should affect the formation of *COCO and *COCHO in a similar manner. Thus, our findings are unlikely to be affected by the cation effect.

Additional mechanisms of C-C bond formation can be conceived if one considers dimerizations of reaction intermediates other than *CO (*e.g.*, $2\,{}^*CHO \longrightarrow {}^*CHOCHO$, or $2\,{}^*CH_2 \longrightarrow C_2H_4$).[16] While thermodynamically feasible, the surface concentration of these intermediates is likely to be too low for such reactions to be important sources of C-C bonds, even if they are

kinetically favored. Therefore, we do not consider C-C bond formation via these pathways.

Before analyzing the ethylene and ethanol paths, let us discuss differences between the CHE and CEP predictions in the overall mechanism. The value of ΔG for the reduction of *CO to *CHO is 0.65 eV, which makes it the most endergonic step in the reaction. The CHE would therefore predict C_2 products to start appearing in sizable quantities at an applied bias of $U \leq -0.65$ V. This agrees well with experiment, where ethylene becomes detectable at potentials between -0.5 and -0.7 V, depending on reaction conditions and specifics of the catalyst.[3] Our CEP calculations confirm that the reaction is downhill ($\Delta G = -0.29$ eV) at $U = -1$ V; the ΔG predicted by the CEP at this potential is only slightly higher than that given by the CHE ($\Delta G = -0.35$ eV). This happens for most of the reactions studied here, *i.e.*, we find that reaction free energies at $U = -1$ V are underestimated by about 0.1 eV by the CHE as compared to the CEP. An exception to this occurs in the reduction of **6a** to **7a**, where the ΔG at -1 V computed with the CHE (-1.72 eV) is higher than that from the CEP (-1.92 eV). This is most likely due to the surface charge destabilizing a double bond to the surface in **6a**.

The dependence of ΔG on voltage appears to be similar for the CEP and CHE: for the *CO + H $\longrightarrow$ *CHO reaction, we calculated ΔG to be 0.78 and 0.24 eV at 0 and -0.5 V, respectively, with the CEP, compared to 0.65 and 0.15 eV with the CHE. Larger discrepancies between the CEP and the CHE can be observed if one considers as an initial state the adsorbate plus an adsorbed hydrogen atom, with the latter being transferred to the former in the final state; this was demonstrated by Goodpaster *et al.*[21] However, this discrepancy is in large part due to the fact that electron transfer has already occurred when the proton is adsorbed at the surface, sharply diminishing the potential dependence. Note also that the results of the CEP are determined not only by the potential and electrolyte concentration, but also by the pH through the dependence of the RHE on pH, as well as the chemical potentials of water and the hydroxide ion. In contrast, the CHE free energies do not depend on the electrolyte concentration or pH. Nonetheless, experiments indicate

that these two factors affect the product distribution of the CO_2RR on copper.[70] Likewise, the CHE cannot predict the voltage dependence shown in Fig. 2 for the CO dimerization process.

Path and selectivity towards ethanol. The analysis above strongly suggests that *COCHO (**3** in Fig. 1) is of pivotal importance in the generation of C_2 compounds. We now propose that this same intermediate is key in determining selectivity between the two major C_2 products of the reaction, ethylene and ethanol. In the pathway presented in Fig. 1, formation of *COCHOH (**4a**) leads to ethylene, whereas glyoxal (ethanedial, **4b**) is eventually reduced to acetaldehyde and ethanol at low and high potentials, respectively. Experimentally, depending on reaction conditions, the amount of ethylene produced is typically about five times that of ethanol,[3] which corresponds to a difference in activation free energies of less than 0.1 eV. The barriers computed here favor the ethylene path by 0.22 eV at $U = 0$ V and also at $U = -1$ V using the CHE ($U_0 = -0.17$ eV, so that the activation free energies are 0.36 and 0.58 for **4a** and glyoxal, respectively), and 0.09 eV at $U = -1$ V using the CEP. These numbers show good consistency between the CHE and CEP barriers, although the CEP predicts a ratio of ethylene to ethanol closer to that often seen in experiments: about $5,000$ for the CHE *vs* 30 for the CEP (one should note, however, that these ratios are extremely sensitive to small changes in the activation energy). A better agreement with experiment is obtained if we take into consideration the tautomerization barrier from **4a** to **5a**. This tautomerization is aided by water and including two explicit water molecules we find that the activation free energy barrier is only 0.19 eV. From the energetic span model,[71] the predicted turnover frequency from **3** to **5** is about 1.63×10^4 s^{-1}, corresponding to an effective $\Delta G^\ddagger$ of 0.51 eV and a ratio $C_2H_4/C_2H_5OH \approx 15$. Considering the limitations in accuracy of semilocal functionals and implicit solvation models, the agreement with experiment is quite reasonable; the mechanism and calculated barriers correctly predict qualitative features such as the preference for ethylene and appearance of glyoxal. Indeed, glyoxal has been proposed to be an intermediate in the CO_2RR[3,13] and is one of the seven C_2 species

that have been detected experimentally.[3]

The fact that glyoxal is a minor product can also be explained by our mechanism: glyoxal is readily consumed because the steps that follow in the reaction are thermodynamically favorable (see Fig. 1). It is likely that most of the glyoxal produced does not leave the surface during the reaction, as it would otherwise be either detected in larger quantities or diffuse away, making it unlikely to reach the surface again. Calculated adsorption energies support this hypothesis: *cis*-glyoxal is favorably chemisorbed on the surface by −0.28 eV, and even more so at high potentials (−0.51 eV at $U = -1$ V). Although calculations done with the RPBE functional predict gas-phase glyoxal to be more stable in the *trans* configuration by 0.19 eV (in agreement with experiments and high-level calculations[72,73]), this difference decreases to 0.1 eV in the electrolyte, according to our simulations. The greater stability of *cis*-glyoxal on the surface is a consequence of both oxygen atoms bonding with the surface, while the carbon atoms form a C=C double bond. This electronic rearrangement is reflected in a shortening of the C-C bond length of glyoxal from 1.55 Å when free to 1.38 Å when adsorbed at the surface. The adsorption of glyoxal is one of the cases where PBE and RPBE yield significantly different results: calculations made using the PBE functional predict a chemisorption energy that is 0.5 eV lower than the value computed using the RPBE functional. This is not surprising if we consider that the PBE functional typically exaggerates the binding energy of oxygen to metal surfaces by about 0.47 eV, and that the RPBE functional was designed to remedy this tendency.[31]

One of the reasons why glyoxal has been proposed to be a CO_2RR intermediate is that it can be reduced to acetaldehyde and ethanol on copper.[3,13] The same is true for glycolaldehyde (2-hydroxyethanal), which is thought to be part of the pathway by which glyoxal is reduced because both molecules produce acetaldehyde at $U < -0.4$ V and ethanol at $U < -0.6$ V.[13] Like glyoxal, glycolaldehyde and acetaldehyde are minor products of copper-catalyzed CO_2 reduction.[3] Acetaldehyde reduction experiments also suggest that this C_2 compound is an intermediate on the pathway to ethanol.[22] Our mechanism can account for all of these

observations as it produces glycolaldehyde from glyoxal, which is further reduced to acetaldehyde, at low potentials, and ethanol, at high potentials. In fact, the CHE predicts ethanol formation to become favorable at $U < -0.46$ V, in rather good agreement with experimental observations. The CEP confirms that reduction of acetaldehyde to ethanol is preferred by -0.56 eV at $U = -1$ V, which explains why the latter is produced in substantially larger quantities than the former: at the typical reaction conditions[3] needed for producing C_2 species in measurable amounts, reduction of acetaldehyde is thermodynamically favored.

A related experimental observation is that, while glyoxal and glycolaldehyde are reduced to other C_2 products on copper, ethylene glycol (ethane-1,2-diol) is not reduced under the same conditions.[13] Therefore, ethylene glycol cannot be an intermediate on the pathway to ethanol, even though it is a minor reaction product.[3] So far, however, no satisfactory explanation has been provided for why ethylene glycol is not reduced by copper while similar compounds are. Therefore, we studied the adsorption energies and geometries of these compounds and found that, particularly at high potentials, the OH groups are repelled by the surface, whereas sp^2 hybridized oxygen atoms have substantial binding with copper. As discussed above, glyoxal bonds with the surface through both carbonyl oxygen atoms; albeit weakly, glycolaldehyde binds through its lone sp^2 oxygen. Both molecules have a Cu-O distance of approximately 2.0 Å. In contrast, attempting to optimize the structure of ethylene glycol attached to Cu(100) results in the adsorbate being driven away from the surface (Cu-O distance of ≈ 3.0 Å), which implies that the adsorption process is endergonic. Hence, as ethylene glycol is produced, it leaves the surface and does not readsorb. Even at high concentrations, we suggest that it does not undergo reduction on copper because it is not chemisorbed.

As an example of how the surface charge can affect the stability of adsorbates with significant dipole moments (*e.g.*, repelling OH groups), consider a reaction alternative to that of $^*CH_2CHOH$ to $^*CH_2CH_2OH$ (**9b** to **10b** on Fig. 1) where the second carbon atom is hydrogenated instead (*i.e.*, $^*CH_2CHOH \longrightarrow {}^*CH_3CHOH$; see Scheme 2). This reaction is

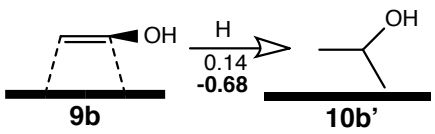

Scheme 2: Alternative reduction step for vinyl alcohol.

thermodynamically uphill by 0.14 eV at $U = 0$ V (CHE). Thus, the CHE would predict the reaction to be exergonic by 0.86 eV at $U = -1$ V, but the CEP predicts a ΔG of only -0.68 eV due to adverse alignment of the adsorbate dipole moment with the charged surface. In contrast, the dipole moment alignment in **10b** is more favorable, and the agreement between the CEP and CHE models is more reasonable, both yielding ΔG values very close to -1 eV (-1.03 and -0.99 eV for the CHE and CEP, respectively). We note in passing that a third alternative reaction is possible starting from **9b**, hydrogen addition to the oxygen atom to form water and $^*CHCH_2$. However, we estimate the barrier for this process to be around 1.5 eV at 0 V, according to the CHE. Consistent with this finding, ethylene has not been observed as a product of glyoxal reduction.[13,69] Therefore, we conclude that $^*CH_2CH_2OH$ is is the direct precursor to ethanol.

To this point, we have used our calculations along with reported experimental observations to argue for the ethanol path shown in Fig. 1. The next step is to compare our findings with those reported in previous theoretical studies. Our work agrees with that by Cheng *et al.*[17] concerning the role of vinyl alcohol (**9b**) as the precursor of acetaldehyde and ethanol. This conclusion is also in accordance with what has been deduced from experimental studies, namely that enol-like species may be key intermediates in the pathway to multicarbon products.[3] Nonetheless, there are differences in the ethanol pathways proposed here and in the work by Cheng *et al.*[17] The mechanism described in that work does not include glyoxal and glycolaldehyde as intermediates to acetaldehyde and ethanol (this is true also for the ethanol pathway suggested by Ledezma *et al.*[22]). In addition, **9b** is not reduced to **10b**, but rather to $^*CH_3CHOH$ (**10b'**). However, as discussed above, the effect of the surface charge is to stabilize **10b** relative to **10b'** (see Scheme 2 and Fig. 1), and the calculated barrier to form $^*CH_3CHOH$ from **9b** is rather high (1.04 eV).[17]

Luo *et al.*[16] propose various alternative, but converging, routes to ethanol. One of them incorporates glyoxal as an intermediate, but not glycolaldehyde, vinyl alcohol, or acetaldehyde. Starting from glyoxal, their mechanism bifurcates from the one proposed here at species **6b**, which loses water to form a cyclic surface species instead of forming glycolaldehyde. Reduction of this species leads to **8b'** (Scheme 3), which we calculate to be 0.42 eV less stable than **8b**, the precursor to vinyl alcohol (**9b**) in Fig. 1. Also, the mechanism and

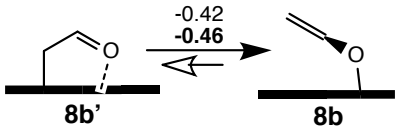

Scheme 3: Isomerization of **8b**.

barriers calculated by Luo *et al.*[16] suggest that glyoxal reduction would produce ethylene, but ethylene has not been detected in glyoxal reduction experiments.[13,69]

Path to acetate. Acetate is a minor product of the CO_2RR whose mechanism of formation has received little attention. Recent experiments by Birdja and Koper[74] suggest that, at high potentials, the local alkaline environment near the electrode can prompt acetaldehyde to undergo a Cannizzaro-type reaction, yielding ethanol and acetate:

$$2CH_3CHO + OH^- \longrightarrow CH_3COO^- + CH_3CH_2OH. \tag{10}$$

However, by contrast with the above reaction, the observed ratio of these two products is not even: the acetaldehyde reduction experiments of Birdja and Koper produce predominantly acetate.[74] Furthermore, the potentials required to produce acetate from acetaldehyde (≈ -1.5 to -2.0 V *vs* the RHE) are higher than those typical of the CO_2RR. Thus, additional pathways to acetate and ethanol must exist apart from the Cannizzaro mechanism.

In Fig. 1, acetate is shown to originate as a byproduct on the ethylene pathway that arises from isomerization of $^*OCH_2COH$ (**6a**) to a three-membered ring compound attached to the surface (**7c**). Although **7c** avoids formation of a double bond to the surface, as occurs in **6a**, the former is highly strained and hence the latter is energetically preferred by

about 0.5 eV. In contrast, reduction of **6a** to continue down the ethylene pathway is highly exergonic ($\Delta G < -0.7$ eV) even in the absence of an applied bias. Nonetheless, reducing **7c** to form acetic acid is even more favorable ($\Delta G \approx -3$ eV) so that the endergonic step may be overcome by this subsequent exergonic reaction. This may explain why the CO_2RR generates acetate with very low current efficiencies (although oxide-derived copper catalysts can generate this species with higher current efficiencies[75]).

The mechanism that we propose here for acetate formation can be probed experimentally. If the path shown in Fig. 1 is correct, then reducing $^{12}C^{18}O$ should result in acetate having both oxygen atoms ^{18}O labeled (in fact, all oxygen atoms in all C_2 products of the mechanism in Fig. 1 would be ^{18}O labeled). Otherwise, one of the oxygen atoms in the acetate ion must originate from water by a different mechanism. (Note that labeled CO, rather than CO_2, is required due to the exchange of oxygen atoms that occurs when CO_2 reacts with water to form bicarbonate ion.) An alternative route to form acetate that would yield a doubly labeled ^{18}O species can be devised starting from **3** via reduction and cyclization to form acetolactone (Scheme 4). Although acetolactone is not a very stable compound and has not

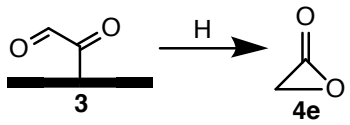

Scheme 4: Formation of acetolactone from *COCHO.

been isolated, it has been detected as a transient species in mass spectroscopy experiments.[76] Two additional reductions and proton transfers could then yield doubly-labeled acetic acid. However, lactones in water easily react to from dicarboxylic acids but oxalic acid (ethanedioic acid) has not been detected as product of the CO_2RR on metallic copper.[3]

Path to ethylene. The path to ethylene is characterized by alternating endergonic and exergonic reactions. All of the endergonic steps involve formation of a radical or double bond to the surface, which is in general not favorable (≈ 0.30–0.44 eV of destabilization). However, the CEP predicts these reactions to be downhill at $U = -1$ V, and the overall reaction is also driven by the subsequent steps which are highly exergonic ($\Delta G > -0.7$ eV). In agreement

with previous experimental and theoretical studies,[13,16,18] one of the intermediates in the mechanism (**9a**) corresponds to adsorbed ethylene oxide (Scheme 5). Like glyoxal in the

Scheme 5: Adsorption of ethylene oxide.

ethanol pathway, ethylene oxide has been suspected to be an intermediate to ethylene because it is readily reduced to this product.[13] Only ethylene is observed in the reduction of ethylene oxide, indicating that the ethylene and ethanol paths do not overlap from the point where ethylene oxide is produced. Thus, we may discard the possibility of **9a** (adsorbed ethylene oxide) being reduced to ethanol based on this experimental observation.

Our route to ethylene generation differs from that proposed by Cheng *et al.*[17] This is because we found *COCHO to be the key intermediate to C_2 products, whereas Cheng *et al.*[17] found that *COCOH leads to ethylene (this is discussed at length in the subsection on C-C bond formation). Our mechanism also differs considerably from that proposed by Luo *et al.*;[16] the only species in common is **9a**. While Luo *et al.*[16] propose that **9a** originates from glyoxal, we discarded this possibility because experimental observations show that glyoxal reduces to ethanol but not ethylene,[13,69] and ethylene oxide reduces to ethylene but not ethanol.[13] In addition, the path to **9a** proposed by Luo *et al.*[16] involves **8b'**, which we calculate to be less stable than **8b** (see Scheme 3). It also interesting to note that while we predict the formation of ethylene from **9a** to be exergonic ($\Delta G = -0.75$ eV), this value is slightly endergonic ($\Delta G = 0.05$ eV) in the work by Luo *et al.*[16] This difference can be traced to the exaggerated adsorption energies of the PBE functional and solvation effects, including the reduction in translational and rotational entropy by the solvent (see Theory and Methods section). (For other reactions not involving adsorption processes, such drastic energy disagreements are not observed: *e.g.*, for $^*\mathrm{CO} + \mathrm{H} \longrightarrow {}^*\mathrm{CHO}$ the difference in the values of ΔG at 0 V *vs* the RHE calculated here and by Luo *et al.*[16] is only 0.03 eV.)

Conclusions

We have used DFT and the CEP model in conjunction with analysis of experimental data reported in the literature to deduce a mechanism for the electrochemical reduction of CO_2 to C_2 products on copper. The mechanism explains several important observations from experiments, including: (1) the difference in activity between the (100) and (111) facets of copper; (2) the seven C_2 species detected; (3) ethanol and ethylene being the major products at typical experimental conditions; (4) the preference of ethylene over ethanol, (5) the reduction of glyoxal and glycolaldehyde to acetaldehyde (at low potentials) and ethanol (at high potentials); (6) the reason why ethylene glycol is not reduced if fed into the reaction; (7) and the reduction of ethylene oxide into ethylene. An experiment to probe the pathway to acetate has also been proposed.

To the best of our knowledge, this is the first theoretical study of CO_2RR using the fixed electrode potential (CEP) model that goes beyond the steps of C-C bond formation to describe pathways for all of the C_2 products that have been detected experimentally. Most of the differences found between this and previous studies were traced to the fact that the latter do not incorporate the charge from the applied potential on the surface, leading to discrepancies for adsorbates with high dipole moments, or to the use of the RPBE functional *vs* the PBE functional, when adsorption processes are involved. While the present approach contains a number of simplifications (limitations of the RPBE functional, lack of explicit solvent and ions, *etc.*), the agreement with experimental information is encouraging and suggests that the simplifications needed in our approach are not critical.

The mechanism proposed here identifies *COCHO (**3**) as the key intermediate for generating C_2 compounds and also for determining selectivity between ethylene and ethanol. This finding paves the way for further theoretical studies aimed at the discovery of catalysts that improve selectivity by analyzing the stabilities and activation barriers of the intermediates involved in the bifurcation process on different surfaces or under different reaction conditions. Investigations of this sort are part of our planned future work. We believe that

this study will be helpful to both theorists and experimentalists working on the mechanism of CO_2 reduction over metallic catalysts and for the design of improved CO_2RR catalysts.

Acknowledgement

This material is based on work performed in the Joint Center for Artificial Photosynthesis, a DOE Energy Innovation Hub, supported through the Office of Science of the U.S. Department of Energy under Award DE-SC00004993. The computational work presented here was carried out at the National Energy Research Scientific Computing Center, a DOE Office of Science User Facility supported by the Office of Science of the U.S. Department of Energy under Contract No. DE-AC02-05CH11231.

References

(1) Hori, Y.; Kikuchi, K.; Murata, A.; Suzuki, A. *Chem. Lett.* **1986**, *15*, 897–898.

(2) Hori, Y.; Murata, A.; Takahashi, R. *J. Chem. Soc., Faraday Trans. 1* **1989**, *85*, 2309–2326.

(3) Kuhl, K. P.; Cave, E. R.; Abram, D. N.; Jaramillo, T. F. *Energy Environ. Sci.* **2012**, *5*, 7050–7059.

(4) Hori, Y.; Wakebe, H.; Tsukamoto, T.; Koga, O. *Surf. Sci.* **1995**, *335*, 258–263.

(5) Takahashi, I.; Koga, O.; Hoshi, N.; Hori, Y. *J. Electroanal. Chem.* **2002**, *533*, 135–143.

(6) Hori, Y.; Takahashi, I.; Koga, O.; Hoshi, N. *J. Mol. Catal. A: Chem.* **2003**, *199*, 39–47.

(7) Whipple, D. T.; Kenis, P. J. A. *J. Phys. Chem. Lett.* **2010**, *1*, 3451–3458.

(8) Peterson, A. A.; Abilda-Pedersen, F.; Studt, F.; Rossmeisl, J.; Norskov, J. K. *Energy Environ. Sci.* **2010**, *3*, 1311–1315.

(9) Nie, X.; Esopi, M. R.; Janik, M. J.; Asthagiri, A. *Angew. Chem., Int. Ed.* **2013**, *52*, 2459–2462.

(10) Kortlever, R.; Shen, J.; Schouten, K. J. P.; Calle-Vallejo, F.; Koper, M. T. M. *J. Phys. Chem. Lett.* **2015**, *6*, 4073–4082.

(11) Baruch, M. F.; Panderill, J. E.; White, J. L.; Bocarsly, A. B. *ACS Catal.* **2015**, *5*, 3148–3156.

(12) Figueiredo, M. C.; Ledezma-Yanez, I.; Koper, M. T. M. *ACS Catal.* **2016**, *6*, 2382–2392.

(13) Schouten, K. J. P.; Kwon, Y.; van der Ham, C. J. M.; Qin, Z.; Koper, M. T. M. *Chem. Sci.* **2011**, *2*, 1902–1909.

(14) Cheng, T.; Xiao, H.; Goddard III, W. A. *J. Phys. Chem. Lett.* **2015**, *6*, 4767–4773.

(15) Cheng, T.; Xiao, H.; Goddard III, W. A. *J. Am. Chem. Soc.* **2016**, *138*, 13802–13805.

(16) Luo, W.; Nie, X.; Janik, M. J.; Asthagiri, A. *ACS Catal.* **2016**, *6*, 219–229.

(17) Cheng, T.; Xiao, H.; Goddard III, W. A. *Proc. Natl. Acad. Sci. U.S.A.* **2017**, *114*, 1795–1800.

(18) Calle-Vallejo, F.; Koper, M. T. M. *Angew. Chem. Int. Ed.* **2013**, *52*, 7282–7285.

(19) Montoya, J. H.; Peterson, A. A.; Nørskov, J. K. *ChemCatChem* **2013**, *5*, 737–742.

(20) Montoya, J. H.; Shi, C.; Chan, K.; Norskov, J. K. *J. Phys. Chem. Lett.* **2015**, *6*, 2032–2037.

(21) Goodpaster, J. D.; Bell, A. T.; Head-Gordon, M. *J. Phys. Chem. Lett.* **2016**, *7*, 1471–1477.

(22) Ledezma-Yanez, I,; Pérez Gallent, E.; Koper, M. T. M.; Calle-Vallejo, F. *Catal. Today.* **2016**, *262*, 90–94.

(23) Favaro, M.; Xiao, H.; Cheng, T.; Goddard III, W. A.; Yano, J.; Crumlin, E. J. *Proc. Natl. Acad. Sci. U.S.A.* **2017**, *114*, 6706–6711.

(24) Xiao, H.; Goddard III, W. A.; Cheng, T.; Liu, Y. *Proc. Natl. Acad. Sci. U.S.A.* **2017**, *114*, 6685–6688.

(25) Mistry, H.; Choy, Y.-W.; Bagger, A.; Scholten, F.; Bonifacio, C. S.; Sinev, I.; Divins, N. J.; Zegkinoglou, I.; Sang Yeon, H.; Kisslinger, K.; Stach, E. A.; Yang, J. C.; Rossmeisl, J.; Roldan Cuenya, B. *Angew. Chem. Int. Ed.* **2017**, *56*, 11552–11556.

(26) Rysuke, J.; Anderson, A. B. *Phys. Rev. B* **2008**, *77*, 245417.

(27) Li, C. W.; Ciston, J.; Kanan, M. W. *Nature* **2014**, *508*, 504–507.

(28) Kwon, Y.; Lum, Y. Clark, E. L.; Ager, J. W.; Bell, A. T. *ChemElectroChem* **2016**, *3*, 1012–1019.

(29) Song, Y.; Peng, R.; Hensley, D. K.; Bonnesen, P. V.; Liang, L.; Wu, Z.; Meyer, H. M.; Chi, M.; Ma, C.; Sumpter, B. G.; Rondinone, A. J. *ChemistrySelect* **2016**, *1*, 6055–6061.

(30) Kresse, G.; Furthmüller J. *Phys. Rev. B* **1996**, *54*, 11169.

(31) Hammer, B.; Hansen, L. B.; Nørskov, J. K. *Phys. Rev. B.* **1999**, *59*, 7413–7421.

(32) Henkelman, G.; Uberuaga, B. P.; Jónsson, H. *J. Chem. Phys.* **2000**, *113*, 9901–9904.

(33) Sheppard, D.; Xiao, P.; Chemelewski, W.; Johnson, D. D.; Henkelman, G. *J. Chem. Phys.* **2012**, *136*, 074103.

(34) Henkelman, G.; Jónsson, H. *J. Chem. Phys.* **1999**, *111*, 7022.

(35) Mathew, K. Henning, R. G. **2016**, arXiv:1601.03346 [cond-mat.mtrl-sci].

(36) Mathew, K.; Sundararaman, R. Letchworth-Weaver, K.; Arias, T. A.; Hennig, R. G. *J. Chem. Phys.* **2014**, *140*, 084106.

(37) Letchworth-Weaver, K.; Arias, T. A. *Phys. Rev. B* **2012**, *86*, 075140.

(38) Sumimoto, M.; Iwane, N.; Takahama, T.; Sakaki, S. *J. Am. Chem. Soc.* **2004**, *126*, 10457–10471.

(39) Liu, C. T.; Maxwell, C. I.; Edwards, D. R.; Neverov, A. A.; Mosey, N. J.; Brown, R. S. *J. Am. Chem. Soc.* **2010**, *132*, 16599–16609.

(40) Nørskov, J. K.; Rossmeisl, J.; Logadottir, A.; Lindqvist, L.; Kitchin, J. R.; Bligaard, T.; Jónsson, H. *J. Phys. Chem. B* **2004**, *108*, 17886–17892.

(41) Akhade, S. A.; Bernstein, N. J.; Esopi, M. R.; Regula, M. J.; Janik, M. J. *Catal. Today* **2017**, *288*, 63–73.

(42) Borukhov, I.; Andelman, D.; Orland, H. *Phys. Rev. Lett.* **1997**, *46*, 435.

(43) Borukhov, I.; Andelman, D.; Orland, H. *Electrochim. Acta* **2000**, *46*, 221–229.

(44) Jinnouchi, R.; Anderson, A. B. *J. Phys. Chem. C* **2008**, *112*, 8747–8750.

(45) Shannon, R. D. *Acta Crystallogr. A* **1976**, *32*, 751–767.

(46) Jenkins, H. D. B.; Thakur, K. P. *J. Chem. Educ.* **1979**, *56*, 576.

(47) Garcia-Ratés, M.; López, N. *J. Chem. Theory Comput.* **2016**, *12*, 1331–1341.

(48) Zhan, C.-G.; Dixon, D. A. *J. Phys. Chem. A* **2002**, *106*, 9737–9744.

(49) Hori, Y.; Murata, A.; Takahashi, R.; Suzuki, S. *J. Am. Chem. Soc.* **1987**, *109*, 5022–5023.

(50) Hori, Y.; Takahashi, R.; Yoshinami, Y.; Murata, A. *J. Phys. Chem. B* **1997**, *101*, 7075–7081.

(51) Gattrell, M.; Gupt, N.; Co, A. *J. Electroanal. Chem.* **2006**, *594*, 1–19.

(52) Nie, X.; Luo, W.; Janik, M. J.; Asthagiri, A. *J. Catal.* **2014**, *312*, 108–122.

(53) Tracy, J. C. *J. Chem. Phys.* **1972**, *56*, 2748–2754.

(54) Akhade, S. A.; McCrum, I. T.; Janik, M. J. *J. Electrochm. Soc.* **2016**, *163*, F477–F484.

(55) Koper, M. T. M. *Chemical Science* **2013**, 4, 2710–2723.

(56) Schouten, K. J.; Qin, Z.; Pérez Gallent, E.; Koper, M. T. *J. Am. Chem. Soc.* **2012**, *134*, 9864–9867.

(57) Schouten, K. J. P.; Pérez Gallent, E.; Koper, M. T. M. *J. Electroanal. Chem.* **2013**, 6–9.

(58) Schouten, K. J.; Pérez Gallent, E.; Koper, M. T. M. *ACS Catal.* **2013**, *3*, 1292–1295.

(59) Chan, K.; Nørskov, J. K. *J. Phys. Chem. Lett.* **2015**, *6*, 2663–2668.

(60) Ou, L.; Long, W.; Chen, Y.; Jin, J. *RSC Adv.* **2015**, *5*, 96281–96289.

(61) Li, H.; Li, Y.; Koper, M. T. M.; Calle-Vallejo, F. *J. Am. Chem. Soc.* **2014**, *136*, 15694–15701.

(62) Baricuatro, J. H.; Ehlers, C. B.; Cummins, K. D.; Soriaga, M. P.; Stickney, J. L.; Kim, Y.-G. *J. Electroanal. Chem.* **2014**, *716*, 101–105.

(63) Kim, Y.-G.; Soriaga, M. P. *J. Electroanal. Chem.* **2014**, *734*, 7–9.

(64) Kim, Y.-G.; Javier, A.; Baricuatro, J. H.; Soriaga, M. P. *Electrocatalysis* **2016**, *7*, 391–399.

(65) Beverskog, B.; Puigdomenech, I. *J. Electrochem. Soc.* **1997**, *144*, 3476–3483.

(66) Gajdoŝ, M.; Hafner, J. *Surf. Sci.* **2005**, *590*, 117–126.

(67) Pérez-Gallent, E.; Figueiredo, M. C.; Calle-Vallejo, F.; Koper, M. T. M. *Angew. Chem. Int. Ed.* **2017**, *56*, 3675–3678.

(68) Pérez-Gallent, E.; Marcandalli, G.; Costa Figueiredo, M.; Calle-Vallejo, F.; Koper, M. T. M. *J. Am. Chem. Soc.* **2017**, *139*, 16412–16419.

(69) Resasco, J.; Chen, L. D.; Clark, E.; Tsai, C.; Hahn, C.; Jaramillo, T. F.; Chan, K.; Bell, A. T. *J. Am. Chem. Soc.* **2017**, *139*, 11277–1287.

(70) Schouten, K. J. P.; Pérez Gallent, E.; Koper, M. T. M. *J. Electroanal. Chem.* **2014**, *716*, 53–57.

(71) Kozuch, S.; Shaik, S. *Acc. Chem. Res.* **2010**, *44*, 101–110.

(72) Butz, K. W.; Johnson, J. R.; Krajnovich, D. J.; Parmenter, C. S. *J. Chem. Phys.* **1987**, *86*, 5923–5939.

(73) Scuseria, G. E.; Schaefer, H. F. *J. Am. Chem. Soc.* **1989**, *111*, 7761–7765.

(74) Birdja, Y. Y.; Koper, M. T. M. *J. Am. Chem. Soc.* **2017**, *139*, 2030–2034.

(75) Bertheussen, E.; Verdaguer-Casadevall, A.; Ravasio, D.; Montoya, J. H.; Trimarco, D. B.; Roy, C.; Meier, S.; Wendland, J.; Nørskov, J. K.; Stephens, I. E. L.; Chorkendorff, I. *Angew. Chem. Int. Ed.* **2016**, *55*,1450–1454.

(76) Schröder, D.; Goldberg, N.; Zummack, W.; Schwarz, H. Poutsma, J. C.; Squires, R. R. *Int. J. Mass Spectrom.*, **1997**, *165*, 71–82.

Graphical TOC Entry